New Journal of Physics
The open access journal at the forefront of physics

Deutsche Physikalische Gesellschaft DPG IOP Institute of Physics

PAPER • OPEN ACCESS

An ion trap source of cold atomic hydrogen via photodissociation of the BaH^+ molecular ion

To cite this article: S A Jones 2022 *New J. Phys.* **24** 023016

New Journal of Physics
The open access journal at the forefront of physics

Deutsche Physikalische Gesellschaft DPG
IOP Institute of Physics

Published in partnership with: Deutsche Physikalische Gesellschaft and the Institute of Physics

OPEN ACCESS

RECEIVED
13 November 2021

REVISED
4 January 2022

ACCEPTED FOR PUBLICATION
26 January 2022

PUBLISHED
16 February 2022

PAPER

An ion trap source of cold atomic hydrogen via photodissociation of the BaH^+ molecular ion

S A Jones*

Department of Physics, Faculty of Science and Engineering, Singleton Park, Swansea University, SA2 8PP Swansea, United Kingdom
* Author to whom any correspondence should be addressed.

E-mail: steven.armstrong.jones@cern.ch

Keywords: hydrogen, antihydrogen, molecular ions, photodissociation, laser cooling, ion traps

Abstract

I present a novel scheme for producing cold (magnetically trappable) atomic hydrogen, based on threshold photodissociation of the BaH^+ molecular ion. BaH^+ can be sympathetically cooled using laser cooled Ba^+ in an ion trap, before it is photodissociated on the single photon $A^1\Sigma^+ \leftarrow X^1\Sigma^+$ transition. The small mass ratio between Ba^+ and BaH^+ ensures a strong overlap within the ion trap for sympathetic cooling, while the large mass ratio between BaH^+ and H means that the released hydrogen can be up to 139 times colder than the parent molecular ions. I examine the hydrogen production rate, and describe how the trap dynamics and photodissociation laser detuning influence the achievable energies. The low infrastructure costs and the ion trap nature of the scheme make it suitable for loading hydrogen into an antihydrogen experiment. This would support a direct matter–antimatter comparison, which could provide important clues as to why our Universe contains so little antimatter.

1. Introduction

The development of quantum mechanics goes hand-in-hand with the study of the hydrogen atom. Hydrogen spectroscopy has been used to determine quantities such as the Rydberg constant [1] and the Lamb shift [2], and remains the go-to tool for testing fundamental physics. The investigation of the proton radius puzzle, a significant disagreement on the charge radius of the proton between different groups using different techniques, is a recent example [3–7].

By comparing it to antihydrogen, hydrogen can be used to test matter–antimatter symmetries with high precision [8]. In the last 10 years, antihydrogen physics has advanced to the point where more than 1000 atoms can be simultaneously trapped [9], cooled [10], and probed with lasers [11, 12] and microwaves [13]. The field is rapidly approaching hydrogen-like precision, and hydrogen–antihydrogen comparisons may soon encounter the same class of hard-to-characterise systematic effects that lead to discrepancies when different groups using different techniques try to measure the same parameters, as demonstrated by the aforementioned proton radius puzzle.

Since ion trap techniques are used to synthesise antihydrogen, an ion trap source of cold atomic hydrogen would be ideal for making a *direct comparison* (i.e. the same experiment in the same trap) between hydrogen and antihydrogen, which would be insensitive to such systematic effects. The superimposed neutral and ion traps would also allow the hydrogen atoms to be detected with high efficiency by using ionisation schemes [14]. For example, a third photon from the 243 nm laser used to drive the two-photon 1s–2s transition is sufficient to ionise the 2s hydrogen atoms. The ions (protons) can be re-trapped and subsequently ejected to a multi-channel plate, with a detection efficiency of 90% [15]. Since this method is charge symmetric between hydrogen and antihydrogen, it avoids systematic effects resulting from how the transition is detected (e.g. quantum interference effects).

It is feasible that such a comparison could exceed the precision of the state-of-the-art hydrogen 1s–2s spectroscopy measurement [16]. Furthermore, it would significantly reduce the amount of time required to

characterise the systematic effects at the 10^{-15} level compared to an antihydrogen-only experiment, which is of considerable benefit given that beam time at CERN is limited.

For this discussion, I define 'cold' hydrogen as hydrogen with a temperature below 0.5 K, since this is the depth of the ALPHA antihydrogen experiment's magnetic minimum trap [9]. To aid comparisons, energies will be expressed in temperature units when applicable using $E = k_B T$, where k_B is the Boltzmann constant.

Traditionally, cold hydrogen has been produced using a single technique: A dilution refrigerator is used to coat a chamber with a film of superfluid helium. Hot atomic hydrogen is then produced via radiofrequency dissociation of H_2, which thermalises via collisions with the chamber to magnetically trappable temperatures [17–19]. Since the technique produces a large quantity of atoms, evaporative cooling can be employed to reduce the temperature of the remaining sample to below 100 μK, even allowing for the formation of Bose–Einstein condensates [20]. However, the requirements of a dilution refrigerator and a superfluid helium coated chamber come with a high infrastructure cost, and make the technique incompatible with the current generation ALPHA experiment.

The photodissociation of cold molecules offers an alternative route to cold hydrogen. By tuning a laser to the dissociation threshold, it is possible to dissociate molecules with less than 50 nK of energy added to the system [21]. Barium hydride (BaH) has been proposed as a candidate, since its large mass means that, upon threshold dissociation, the hydrogen atom will have an energy 139 times lower than the parent molecule [22]. However, this scheme has a number of complications. Firstly, buffer gas cooling is required to pre-cool the internal states of the molecule, which introduces vacuum incompatibilities. Secondly, the molecule must be Doppler cooled to sufficiently low temperatures. Directly laser cooling molecules is challenging, but there has already been progress on this front [23]. Finally, the photodissociation scheme is complex, requiring a two-photon process involving a high power ultra-violet laser, followed by a magnetic field sweep to couple into a Feshbach resonance.

These problems can be mitigated by instead choosing a molecular hydride *ion*. The alkali-earth-metal ions have convenient laser cooling transitions, and can be used to sympathetically cool their corresponding hydride molecular ions in an ion trap. Since the ion trap lifetime is essentially infinite, one can simply wait for the internal states to spontaneously decay, avoiding the need for buffer gas cooling. Photodissociation experiments have been performed with the beryllium hydride molecular ion (BeH^+), which has been sympathetically cooled in a Penning trap using laser cooled Be^+ [24]. BeH^+ has a simple photodissociation scheme, exciting the $B^1\Pi \leftarrow X^1\Sigma^+$ transition with a single photon. In this experiment, the researchers viewed the BeH^+ as a contaminant and dissociated far above the threshold, where a convenient laser was available. The wavelength for threshold photodissociation is around 172 nm, which is difficult to obtain with present laser technologies.

Here, I propose threshold photodissociation of the barium hydride molecular ion (BaH^+), which has been sympathetically cooled in an ion trap using laser cooled Ba^+, as a method for producing cold atomic hydrogen. BaH^+ has a promising energy level structure for threshold photodissociation, and a convenient (visible) photodissociation wavelength around 411 nm. The high mass ratio benefits from the neutral BaH scheme can be exploited in the same manner, while realising the benefits of the ion trap scheme employed for BeH^+ to produce around 0.2 M cold atoms per ~100 s experimental cycle. In the following work, I consider only the most abundant barium isotope, ^{138}Ba.

2. Methods

2.1. Loading and cooling

Large quantities of BaH^+ could be loaded into a trap using laser ablation. Ablation of neutral BaH from a BaH_2 target has been realised using an infra-red laser [25], and it has been shown in general that using an ultra-violet ablation laser increases the ion fraction [26]. Laser ablation has been demonstrated as a viable technique for loading Be^+ into the ALPHA antihydrogen experiment without degrading the quality of the vacuum [27]. It is likely that some of the hot BaH^+ resulting from ablation will either predissociate through a repulsive electronic state or be directly dissociated by the ablation process to yield a mix of Ba^+ and BaH^+. If not, then hot (above threshold) photodissociation can be performed until a suitable ratio of Ba^+ to BaH^+ for sympathetic cooling is achieved. Ba^+ is cooled on the 493 nm $6s_{1/2}$–$6p_{1/2}$ transition, and requires a repump laser at 650 nm to address the $6p_{1/2}$–$5d_{3/2}$ decay pathway [28].

2.2. Electronic and vibrational states

BaH^+ has a single bound ground orbital ($X^1\Sigma^+$) which has an asymptote given by the $Ba^+(6s) + H(1s)$ atomic levels, and several excited orbital configurations which have asymptotes given by the metastable $Ba^+(5d) + H(1s)$ atomic levels. Conveniently, only the $A^1\Sigma^+ \leftarrow X^1\Sigma^+$ transition is allowed, since transitions to the triplet and Δ states are dipole forbidden, and the $B^1\Pi \leftarrow X^1\Sigma^+$ transition has a negligible

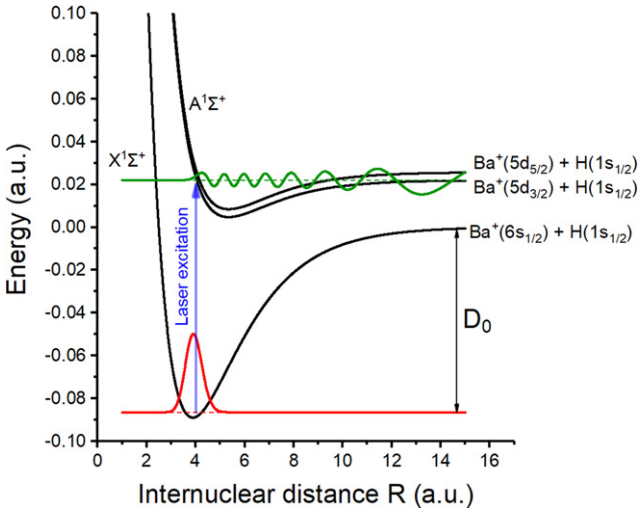

Figure 1. Morse potentials representing the $X^1\Sigma^+$ and $A^1\Sigma^+$ electronic orbitals of BaH^+ are shown in black. The calculated ground vibrational state (red) and the dissociation threshold (green) wavefunctions are plotted. The photodissociation transition is shown in blue.

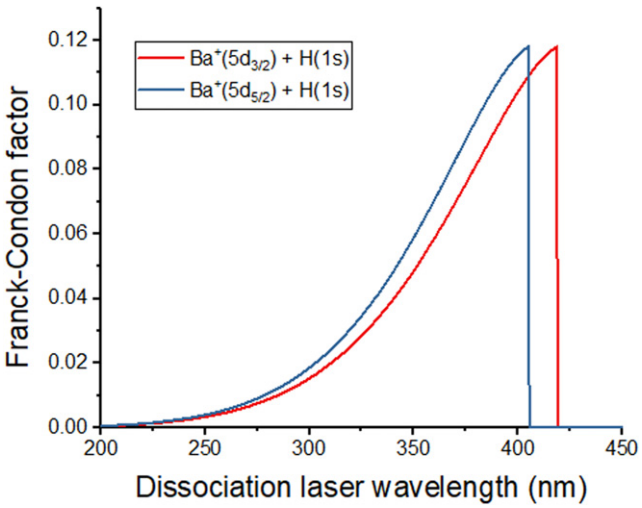

Figure 2. The Franck–Condon factors above the dissociation threshold for the molecular potentials corresponding to the $Ba^+(5d_{3/2}) + H(1s)$ (red) and $Ba^+(5d_{5/2}) + H(1s)$ (blue) asymptotes are calculated.

Franck–Condon factor [29–34]. Figure 1 shows the potentials for the $X^1\Sigma^+$ and $A^1\Sigma^+$ orbitals. For simplicity, these have been approximated using Morse potentials [35] tuned to match the potentials predicted by *ab initio* calculations [29–34]. The wavefunctions of the ground vibrational state (red) and the $A^1\Sigma^+$ threshold (green) are calculated and overlaid onto figure 1, and the resulting Franck–Condon factors are presented in figure 2.

There is a large uncertainty associated with the photodissociation transition wavelength, primarily due to the uncertainty in the value of the ground state binding energy $D_0 = D_e - \omega_e/2$. The photodissociation wavelength, given by $\lambda = \{D_0 + E[Ba^+(5d_{3/2}) - Ba^+(6s)]\}/hc$, and the spectroscopic values used to calculate D_0, are shown in table 1. The averaged result from *ab initio* studies of 422 ± 18 nm (1 SD) is in agreement with the single experimental measurement of 411 ± 14 nm [36]. This gives a level of confidence that the photodissociation transition is in the visible or near ultra-violet part of the spectrum, where diode lasers are readily available. Notably, this means that the photodissociation laser and the Ba^+ cooling lasers can be coupled into the experiment through a single optical fibre. This is particularly relevant for Penning trap experiments such as ALPHA, where trap access is often limited.

Upon photodissociation into the $5d_{3/2}$ level, the Ba^+ ions will enter into the cooling/repump cycle and fluoresce, giving a signal that hydrogen has been produced. This signal can be used to identify the transition threshold, since it will have a characteristic sharp onset followed by a slow decay as a function of the

Table 1. The spectroscopic constants used to calculate the BaH^+ photodissociation transition wavelength. The vibrational constant ω_e is not measured in the single experimental reference, so the averaged value from *ab initio* studies is taken. Reference [32] contains two different methods for calculating the spectroscopic constants, labelled a and b.

	Re (a.u.)	D_e (cm^{-1})	ω_e (cm^{-1})	D_0 (cm^{-1}) (calculated)	Transition (cm^{-1}) (calculated)	Transition (nm) (calculated)	Reference
	3.88	195 65	1263.4	18964.3	23838.15	419.50	[29]
	4.07	197 60	1370	190 75	23949.85	417.56	[30]
	3.93	216 04	1368	209 20	25793.85	387.69	[31]
Ab initio calculations	4.053	190 45	1345.8	18372.1	23245.95	430.18	[32][a]
	4.052	197 63	1352.7	19086.65	23960.50	417.35	[32][b]
	4.16	18502.78	1408	17798.78	22672.63	441.06	[33]
	4.04	184 70	1224	178 58	22731.85	439.91	[34]
Average ± 1 S.D.	4.03 ± 0.09	19534 ± 1067	1333 ± 65	18868 ± 1058	23741 ± 1058	422 ± 18	
Experiment		20163 ± 800	1333 ± 65	19496 ± 833	24370 ± 833	411 ± 14	[35]

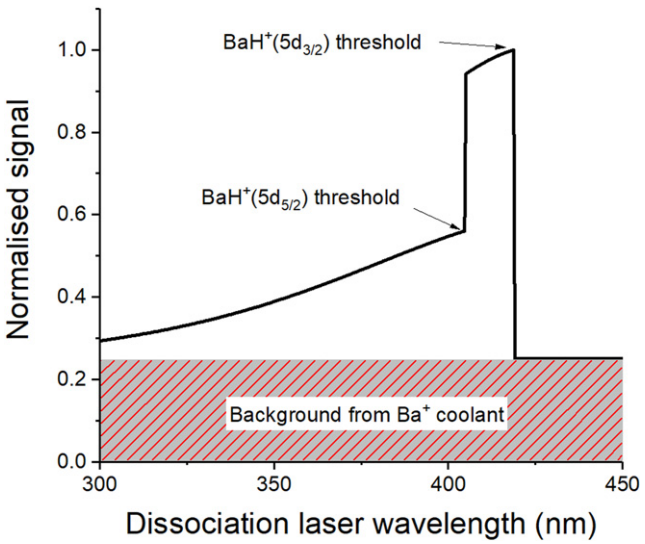

Figure 3. A sketch of the expected spectrum of a photodissociation experiment with BaH^+. Upon photodissociation, Ba^+ released in the $5d_{3/2}$ level enters the cooling cycle and fluoresces, producing a detectable signal. There is a constant background from the Ba^+ initially loaded into the trap to sympathetically cool the BaH^+, which contributes 25% of the total signal in this plot. The onset at the right of the plot corresponds to the photodissociation threshold of the $Ba^+(5d_{3/2}) + H(1s)$ asymptote. Once the laser has enough energy to photodissociate to the $Ba^+(5d_{5/2}) + H(1s)$ asymptote, there is a sharp drop in the signal, since the $Ba^+(5d_{5/2})$ ions do not enter the cooling cycle and fluoresce, i.e. they are in a dark state.

dissociation laser wavelength. The Ba^+ ions produced by photodissociation into the $5d_{5/2}$ level are not repumped, and thus do not enter the cooling cycle. An example spectrum one might measure from a spectroscopy experiment, taking into account this behaviour, is shown in figure 3. The feature is broad enough that an initial search could be made using spectrally filtered LEDs, before utilising laser spectroscopy to find the threshold. High lying vibrational states of the $5d_{5/2}$ manifold may be visible within the feature as dark lines.

Transition dipole moments vary in molecules as a function of the internuclear distance R. The transition dipole moment for the $A^1\Sigma^+ \leftarrow X^1\Sigma^+$ transition in BaH^+ has been calculated by Aymar and Dulieu [31], and crosses through zero close to the internuclear distance corresponding to threshold photodissociation (R_{21}). If we assume the worst-case scenario; the transition dipole moment crosses through zero at exactly R_{21}, and the Born–Oppenheimer approximation holds exactly (i.e. that the transition shown in figure 1 must be exactly vertical), the transition rate can be calculated as a function of the dissociation laser detuning. Following the definitions provided by Hilborn [37], the Rabi frequency is given by $\Omega = \mu_{21}F_{21}E_0/\hbar$, where μ_{21} is the transition dipole moment, F_{21} is the Franck–Condon factor, E_0 is the electric field amplitude, and $\hbar$ is the reduced Planck's constant. We can then define the excitation time as $\tau = 2\pi/\Omega$. Approximating the transition dipole moment as linear near the zero crossing, for a 100 mW photodissociation laser with a beam waist ($1/e^2$) of 1 mm, the excitation time is plotted against the dissociation laser detuning in figure 4. The hydrogen atom will take most (138/139) of the excess photon energy as kinetic energy, and is expressed in units of temperature on the bottom axis. The transition dipole

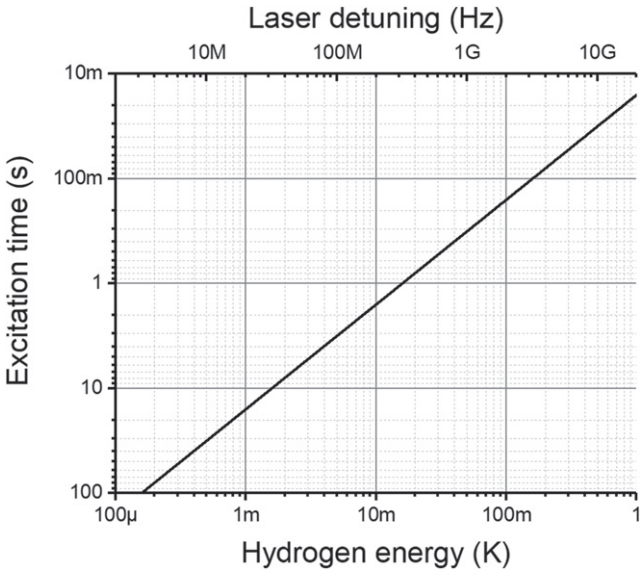

Figure 4. The excitation time required for the photodissociation transition to occur is plotted against the dissociation laser frequency detuning and the energy of the released hydrogen atom, assuming a 100 mW excitation laser with a 1 mm beam waist ($1/e^2$).

moment flattens out at $\mu_{21} = -0.1D$, corresponding to an excitation time of 0.4 μs, and preserving the coarse structure of figure 3.

2.3. Rotational states

So far, the rotational states of the molecular ion have not been considered. The spacing of the rotational levels is much greater than the depth of typical magnetic traps, so hydrogen atoms resulting from only one pair of levels can be trapped. For a $\Sigma \leftarrow \Sigma$ transition, the rotational state must change by $\Delta J = \pm 1$. The rotation of the molecule imposes a centrifugal barrier which must be overcome for photodissociation. Since this extra energy would be converted into kinetic energy upon fragmentation, the $J' = 0 \leftarrow J = 1$ transition should be targeted.

While the electronic and vibrational states of BaH^+ quickly decay to the ground state, the rotational energies are small enough that a broad range of levels will be occupied at room temperature (see figure 5). Performing the experiment in a cryogenic environment, such as that used in antihydrogen experiments ($\sim$10 K), increases the $J = 1$ population fraction to around 44%. For a room temperature experiment, rotational laser cooling can be employed to achieve similar results on a 40–60 s timescale, as demonstrated with MgH^+ [38]. This can be driven by a broad mid infra-red laser at 1250 cm^{-1} [29, 30]. The rotational laser cooling scheme and the photodissociation transition for BaH^+ are presented in figure 6.

2.4. Hyperfine states

Since the angular momentum of the dissociating photon is absorbed by the rotation of the molecule, and dissociation occurs through a singlet state, the resulting Ba^+ and H will be emitted in electron orbital configurations with $m_j = +1/2, -1/2$ or $-1/2, +1/2$. Hydrogen atoms with $m_j = +1/2$ will seek a magnetic minimum, and can hence be trapped, while atoms with $m_j = -1/2$ will seek a high magnetic field and be untrappable, resulting in a 50% trapping efficiency.

The contribution from the spin of the hydrogen nucleus to the $X^1\Sigma^+$ and $A^1\Sigma^+$ molecular orbitals should be comparable. Therefore, hydrogen atoms dissociated into the two low-field seeking magnetic levels $F = 1$, $m_f = +1$ and $F = 1$, $m_f = 0$ will have similar kinetic energies. This also means that the photodissociation transition should be insensitive to external magnetic fields. Note that this would be further simplified for BaD^+, since neither ^{138}Ba or D (^{2}H) have nuclear spin.

3. Trap dynamics

While ion traps have many advantages, they have a key disadvantage. The ions will repel each other due to the Coulomb force, limiting the density of hydrogen atoms that can be produced. Here, we will consider the two most common types of ion traps: Penning traps, which confine particles radially using a solenoid

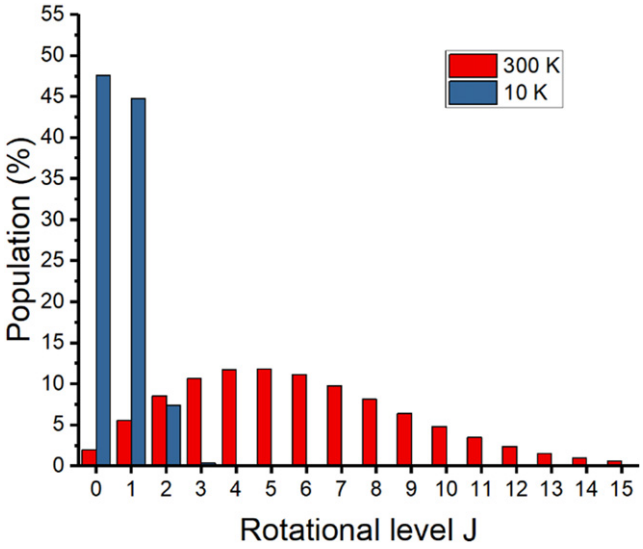

Figure 5. The rotational level population of BaH^+ in the ground electronic and vibrational state at 300 K (red), and 10 K (blue) at thermal equilibrium.

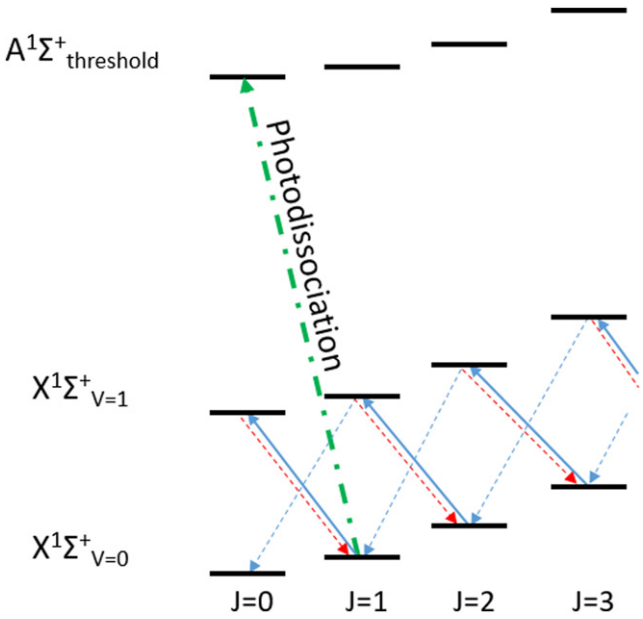

Figure 6. A mid infra-red laser drives $\Delta J = -1$ transitions (solid blue) from the ground to the first excited vibrational level of BaH^+. The level can then decay back to the ground vibrational level via a $\Delta J = -1$ transition (dashed blue), achieving rotational cooling, or via a $\Delta J = +1$ transition (dashed red) to the state of origin. The photodissociation transition is shown in green.

magnetic field, and linear radiofrequency traps, which use an oscillating electric field applied to rod-shaped electrodes to provide the radial confinement. Both traps use a DC potential to confine the particles axially.

3.1. Penning traps

Penning traps are the tool of choice for synthesising antihydrogen. In a Penning trap, the ion plasma will rotate around the trap axis at a frequency proportional to the solenoid field strength, and the mass, charge, and density of the ions. For a mixed species plasma, the different masses can centrifugally separate, with the heavier ions pushed to the outside [39]. BaH^+ ions at higher radii will have higher angular velocities, which will be inherited by the hydrogen atoms upon photodissociation. Furthermore, if the Ba^+ and BaH^+ become spatially separated, the sympathetic cooling power will be reduced.

A Poisson solver was used to find the equilibrium density of a 1 K, 25 mm long plasma consisting of 0.1 M Ba^+ ions and 1 M BaH^+ molecular ions. The solenoid has a field strength of 1 T, and the plasma sits

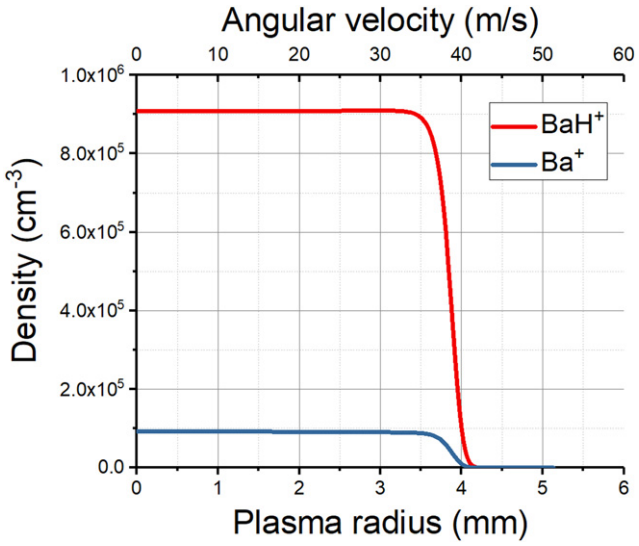

Figure 7. The equilibrium density of a dual species, 25 mm long plasma in a 1 T Penning trap, consisting of 1 M BaH^+ molecular ions (red), and 0.1 M Ba^+ ions (blue). The plasma temperature is 1 K.

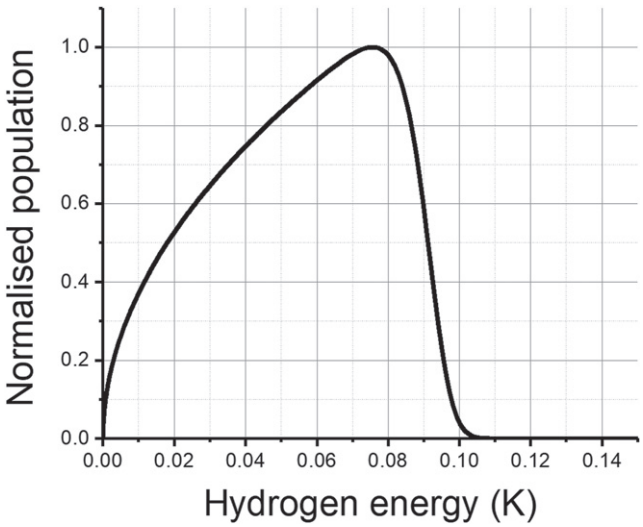

Figure 8. The contribution to the energy distribution of hydrogen atoms released upon threshold photodissociation of the plasma shown in figure 7, due to the plasma rotation.

in a 5 V deep axial potential, typical of the trapping parameters used in ALPHA. As expected from the close mass ratio between Ba^+ and BaH^+ (138:139), we see in figure 7 that the centrifugal separation is negligible.

The velocity of the ions is given by $v = \omega r$, where ω is the plasma rotation frequency. For the plasma simulated in figure 7, $\omega \approx 10$ krad s^{-1}. We can convert the density into a population by integrating under the volume of the plasma. The energy distribution (plotted in figure 8) is then given by $E = 1/2\ m_H v^2$, where m_H is the mass of the hydrogen atom. Note that figure 8 neglects the thermal motion of the ions within the plasma. Even at a relatively warm temperature of 1 K, the large mass ratio between BaH^+ and H of 139:1 means that less than 8 mK is contributed to the dissociated hydrogen. There will also be a Doppler broadening of the photodissociation transition associated with the thermal and rotational motion of the plasma.

There are various techniques that one can employ to reduce the energy distribution, ranging from using a small diameter dissociation laser beam aligned along the trap axis, to holding a large reservoir of ions, from which small scoops can be extracted on axis for photodissociation. For comparisons with antihydrogen, it may be beneficial to laser cool the hydrogen using the same scheme as employed for antihydrogen, to achieve identical thermal distributions.

3.2. Radiofrequency traps

While radiofrequency traps have not yet been used to synthesise antihydrogen, they are commonplace in the ion trapping community, and have a wide array of applications. Indeed, there exists a proposal which shares many similarities with this scheme to sympathetically cool the positive antihydrogen ion in a radiofrequency trap, before removing the extra positron to produce ultracold antihydrogen [40]. The GBAR collaboration at CERN has ongoing efforts to realise this.

Since radiofrequency traps do not require a magnetic field, laser cooling of Ba^+ is simplified, as additional frequencies are not required to address Zeeman sub-levels. For a linear radiofrequency trap, the dependence of particle motion on the produced hydrogen resembles that of the Penning trap—the ions at higher radii experience a higher velocity. In this case, it is due to increased micromotion from the applied oscillating field. A preliminary study by Poljakov shows that radiofrequency traps are also viable tools for producing cold hydrogen via photodissociation of BaH^+ [41].

In contrast to Penning traps, one can tailor the radial potential by increasing the number of electrodes. A higher order multipole trap gives a flatter potential near the centre, which would allow for production of colder hydrogen further from the trap axis.

3.3. Hydrogen traps

By superimposing a Ioffe magnetic trap with the ion trap, low-field seeking hydrogen atoms created inside the trap will be confined. Higher order magnetic multipole traps are preferred, since they will have a greater critical radius at which charged particles will be lost due to diffusion [42]. In ALPHA, which uses an octupole field for radial confinement, the critical radius is around 5 mm. As demonstrated with antihydrogen production at ALPHA [9], the ion trap could be continuously cycled to produce more hydrogen while retaining the magnetic trap, allowing hydrogen to be accumulated.

4. Production rates

We can estimate the hydrogen production rate by considering a simple (yet realistic) experiment. Around 1 M BaH^+ are loaded into a Penning trap, with a sufficient number of Ba^+ to sympathetically cool them. Rotational cooling is employed for 60 s to yield ∼0.44 M BaH^+ in the $J = 1$ rotational state, before the photodissociation transition is driven. Of the produced hydrogen atoms, ∼50% will be in the correct low-field seeking state to be magnetically trapped.

For hydrogen which is cold enough to trap (<0.5 K), the photodissociation laser can be run for 10 s at a detuning of 100 MHz above the threshold, resulting in ∼0.2 M trapped hydrogen atoms per ∼100 s long production cycle. In a more complex experimental setup, where the rotationally cold ions are prepared in parallel or in a large reservoir, the cycle time becomes limited by the excitation time given in figure 4. The slow production rate should be seen as an inconvenience rather than a problem, since the typical lifetime of an ion trap is much greater than 1000 s.

5. Conclusion

A novel scheme for producing cold atomic hydrogen via photodissociation of the BaH^+ molecular ion has been presented. The scheme has a number of key advantages over both historical hydrogen sources, and new sources currently under investigation. It preserves the quality of the vacuum, requires little infrastructure, and avoids complex molecular Doppler cooling and multi-photon dissociation schemes. Although the density and production rate are comparatively low, the ion trap allows for efficient detection of the produced hydrogen.

Notably, the scheme is ideal for loading hydrogen into an antihydrogen experiment for a direct matter–antimatter comparison. It relies on the same ion trapping techniques that are commonplace among the antihydrogen community, and takes advantage of infrastructure which is already in place. Since the production rate is much higher than the antihydrogen production rate (∼20 atoms per 120 s cycle) [9], one can imagine an experiment in which hydrogen is produced in a single cycle and measured in parallel with antihydrogen which has been accumulated over a full day, enabling a direct comparison which is immune to many systematic effects. This would significantly reduce the amount of beam time required to study the systematic effects over an antihydrogen-only experiment, and could result in a relative comparison between hydrogen and antihydrogen which exceeds the state-of-the-art measurements in hydrogen.

A proof of principle experiment could be performed without the magnetic trap and laser systems required for hydrogen spectroscopy, since, upon photodissociation, the co-emitted Ba^+ is captured in the

ion trap and provides a fluorescence signal. This would provide much needed verification of the *ab initio* techniques used for calculating the spectra of molecular systems such as BaH^+.

The scheme could be extended to produce (for example) cold deuterium using BaD^+, and ro-vibrational spectroscopy of such systems may provide interesting tests of fundamental physics.

Acknowledgments

I acknowledge many useful discussions with my colleagues at the ALPHA collaboration. In particular, I would like to thank S Eriksson, N Madsen, and J Nauta for valuable comments on this manuscript. The code used to calculate the Ba^+/BaH^+ Penning trap equilibrium densities was written by F Robicheaux. This work was supported by the EPSRC.

Data availability statement

The data that support the findings of this study are available upon reasonable request from the authors.

ORCID iDs

S A Jones https://orcid.org/0000-0001-8205-2186

References

[1] Pohl R *et al* 2010 The size of the proton *Nature* **466** 213–6
[2] Lamb W E and Retherford R C 1947 Fine structure of the hydrogen atom by a microwave method *Phys. Rev.* **72** 241–3
[3] Beyer A *et al* 2017 The Rydberg constant and proton size from atomic hydrogen *Science* **358** 79
[4] Fleurbaey H, Galtier S, Thomas S, Bonnaud M, Julien L, Biraben F, Nez F, Abgrall M and Guéna J 2018 New measurement of the 1S–3S transition frequency of hydrogen: contribution to the proton charge radius puzzle *Phys. Rev. Lett.* **120** 183001
[5] Bezginov N, Valdez T, Horbatsch M, Marsman A, Vutha A C and Hessels E A 2019 A measurement of the atomic hydrogen Lamb shift and the proton charge radius *Science* **365** 1007
[6] Grinin A, Matveev A, Yost D C, Maisenbacher L, Wirthl V, Pohl R, Hänsch T W and Udem T 2020 Two-photon frequency comb spectroscopy of atomic hydrogen *Science* **370** 1061
[7] Brandt A D, Cooper S F, Rasor C, Burkley Z, Yost D C and Matveev A 2021 Measurement of the $2S_{1/2}$–$8D_{5/2}$ transition in hydrogen (arXiv:2111.08554)
[8] Charlton M *et al* 2020 *Antihydrogen and Fundamental Physics* (*Springer Briefs in Physics*) (New York: Springer) https://doi.org/10.1007/978-3-030-51713-7
[9] Ahmadi M *et al* 2017 Antihydrogen accumulation for fundamental symmetry tests *Nat. Commun.* **8** 681
[10] Baker C J *et al* 2021 Laser cooling of antihydrogen atoms *Nature* **592** 35–42
[11] Ahmadi M *et al* 2018 Characterization of the 1S–2S transition in antihydrogen *Nature* **557** 71–5
[12] The ALPHA Collaboration 2020 Investigation of the fine structure of antihydrogen *Nature* **578** 375–80
[13] Ahmadi M *et al* 2017 Observation of the hyperfine spectrum of antihydrogen *Nature* **548** 66–9
[14] Lenz Cesar C 2016 A sensitive detection method for high resolution spectroscopy of trapped antihydrogen, hydrogen and other trapped species *J. Phys. B: At. Mol. Opt. Phys.* **49** 074001
[15] Fehre K *et al* 2018 Absolute ion detection efficiencies of microchannel plates and funnel microchannel plates for multi-coincidence detection *Rev. Sci. Instrum.* **89** 045112
[16] Parthey C *et al* 2011 Improved measurement of the hydrogen 1S–2S transition frequency *Phys. Rev. Lett.* **107** 203001
[17] Masuhara N, Doyle J, Sandberg J, Kleppner D, Greytak T, Hess H and Kochanski G 1988 Evaporative cooling of spin-polarized atomic hydrogen *Phys. Rev. Lett.* **61** 935–8
[18] Doyle J M, Sandberg J C, Yu I A, Cesar C L, Kleppner D and Greytak T J 1994 Evaporative cooling of atomic hydrogen: theory of cooling and progress towards the Bose–Einstein transition *Physica* B **194–196** 13–4
[19] Pinkse P, Mosk A, Weidemüller M, Reynolds M, Hijmans T and Walraven J 1998 One-dimensional evaporative cooling of magnetically trapped atomic hydrogen *Phys. Rev.* A **57** 4747–60
[20] Fried D, Killian T, Willmann L, Landhuis D, Moss S, Kleppner D and Greytak T 1998 Bose–Einstein condensation of atomic hydrogen *Phys. Rev. Lett.* **81** 3811–4
[21] McGuyer B H, McDonald M, Iwata G Z, Tarallo M G, Grier A T, Apfelbeck F and Zelevinsky T 2015 High-precision spectroscopy of ultracold molecules in an optical lattice *New J. Phys.* **17** 055004
[22] Lane I 2015 Production of ultracold hydrogen and deuterium via Doppler-cooled Feshbach molecules *Phys. Rev.* A **92** 022511
[23] McNally R, Kozyryev I, Vazquez-Carson S, Wenz K, Wang T and Zelevinsky T 2020 Optical cycling, radiative deflection and laser cooling of barium monohydride ($^{138}Ba^1H$) *New J. Phys.* **22** 083047
[24] Sawyer B, Bohnet J, Britton J and Bollinger J 2015 Reversing hydride-ion formation in quantum-information experiments with Be^+ *Phys. Rev.* A **91** 011401
[25] Iwata G, McNally R and Zelevinsky T 2017 High-resolution optical spectroscopy with a buffer-gas-cooled beam of BaH molecules *Phys. Rev.* A **96** 022509
[26] Torrisi L, Gammino S, Andò L, Nassisi V, Doria D and Pedone A 2003 Comparison of nanosecond laser ablation at 1064 and 308 nm wavelength *Appl. Surf. Sci.* **210** 262–73
[27] Baker C J *et al* 2021 Sympathetic cooling of positrons to cryogenic temperatures for antihydrogen production *Nat. Commun.* **12** 6139

[28] Neuhauser W, Hohenstatt M, Toschek P and Dehmelt H 1978 Optical-sideband cooling of visible atom cloud confined in parabolic well *Phys. Rev. Lett.* **41** 233–6
[29] Mejrissi L, Habli H, Ghalla H, Oujia B and Gadéa F 2013 Adiabatic *ab initio* study of the BaH^+ ion including high energy excited states *J. Phys. Chem.* A **117** 5503–17
[30] Allouche A R, Spiegelmann F and Aubert-Frécon M 1993 Theoretical study of the low-lying electronic states of the BaH^+ molecular ion *Chem. Phys. Lett.* **204** 343–9
[31] Aymar M and Dulieu O 2012 The electronic structure of the alkaline-earth-atom (Ca, Sr, Ba) hydride molecular ions *J. Phys. B: At. Mol. Opt. Phys.* **45** 215103
[32] Abe M, Kajita M, Hada M and Moriwaki Y 2010 *Ab initio* study on vibrational dipole moments of *X*H molecular ions: $X = {}^{24}$Mg, ^{40}Ca, ^{64}Zn, ^{88}Sr, ^{114}Cd, ^{138}Ba, ^{174}Yb and ^{202}Hg *J. Phys. B: At. Mol. Opt. Phys.* **43** 245102
[33] Ohanessian G, Brusich M and Goddard W 1990 Theoretical study of transition-metal hydrides: V. Hafnium to mercury (HfH^+ through HgH^+), barium and lanthanum (BaH^+ and LaH^+) *J. Am. Chem. Soc.* **112** 7179–89
[34] Fuentealba P and Reyes O 1987 Pseudopotential calculations on the ground state of the alkaline-earth monohydride ions *Mol. Phys.* **62** 1291–6
[35] Morse P 1929 Diatomic molecules according to the wave mechanics: II. Vibrational levels *Phys. Rev.* **34** 57–64
[36] Armentrout P B and Beauchamp J L 1980 Experimental and theoretical studies of the reaction $Ba^+(D_2, D)BaD^+$: sequential impulse model for endothermic reactions *Chem. Phys.* **48** 315–20
[37] Hilborn R 1982 Einstein coefficients, cross sections, *f* values, dipole moments, and all that *Am. J. Phys.* **50** 982–6
[38] Staanum P *et al* 2010 Rotational laser cooling of vibrationally and translationally cold molecular ions *Nat. Phys.* **6** 271–4
[39] O'Neil T 1981 Centrifugal separation of a multispecies pure ion plasma *Phys. Fluids* **24** 1447–51
[40] Walz J and Hänsch T W 2004 A proposal to measure antimatter gravity using ultracold antihydrogen atoms *Gen. Relativ. Gravit.* **36** 561–70
[41] Poljakov N 2021 Sympathetic cooling of ${}^{139}BaH^+$ using laser-cooled ${}^{138}Ba^+$ in linear RF traps *CERN-STUDENTS-Note-2021-164* CERN
[42] Fajans J, Madsen N and Robicheaux F 2008 Critical loss radius in a Penning trap subject to multipole fields *Phys. Plasmas* **15** 032108